

# Interaction of high density lipoprotein particles with membranes containing cholesterol

Susana A. Sanchez,<sup>1,\*</sup> Maria A. Tricerri,<sup>†</sup> and Enrico Gratton<sup>\*</sup>

Laboratory for Fluorescence Dynamics,<sup>\*</sup> University of California-Irvine, Irvine, CA; and Instituto de Investigaciones Bioquímicas,<sup>†</sup> Facultad de Ciencias Medicas, Universidad Nacional de La Plata, La Plata, Argentina

**Abstract** In this study, free cholesterol (FC) efflux mediated by human HDL was investigated using fluorescence methodologies. The accessibility of FC to HDL may depend on whether it is located in regions rich in unsaturated phospholipids or in domains containing high levels of FC and sphingomyelin, known as “lipid rafts.” Laurdan generalized polarization and two-photon microscopy were used to quantify FC removal from different pools in the bilayer of giant unilamellar vesicles (GUVs). GUVs made of POPC and FC were observed after incubation with reconstituted particles containing apolipoprotein A-I and POPC [78Å diameter reconstituted high density lipoprotein (rHDL)]. Fluorescence correlation spectroscopy data show an increase in rHDL size during the incubation period. GUVs made of two “raft-like” mixtures [DOPC/DPPC/FC (1:1:1) and POPC/SPM/FC (6:1:1)] were used to model liquid-ordered/liquid-disordered phase coexistence. Through these experiments, we conclude that rHDL preferentially removes cholesterol from the more fluid phases. These data, and their extrapolation to in vivo systems, show the significant role that phase separation plays in the regulation of cholesterol homeostasis.—Sanchez, S. A., M. A. Tricerri, and E. Gratton. Interaction of high density lipoprotein particles with membranes containing cholesterol. *J. Lipid Res.* 2007. 48: 1689–1700.

**Supplementary key words** raft mixtures • giant unilamellar vesicles • two-photon microscopy • 6-lauroyl-2-(dimethylamino) naphthalene

It is generally accepted that the chronic, progressive pathologies atherosclerosis and coronary heart disease are characterized by two processes: recruitment of inflammatory cells from the circulation, and accumulation of lipids in the artery wall. An excess of unesterified free cholesterol (FC) is toxic to cells; therefore, several mechanisms triggering its clearance have been identified. Extensive epidemiological research supports a key role of HDLs and their major apolipoprotein A-I (apoA-I) in the prevention of coronary heart disease. Different protective capabilities

have been attributed to HDL (1–3), including their critical participation in cholesterol catabolism.

Human plasma HDLs, a population of particles highly heterogeneous in lipid and apolipoprotein composition as well as size and shape, are the main cholesterol acceptors in vivo. In particular, recent research has shown that a nascent subspecies of HDL, pre $\beta$ -HDL, containing apoA-I as its sole protein moiety, removes lipids very efficiently from cells (4), interacts with LCAT (5), and undergoes further metabolism to yield mature circulating spherical lipoproteins.

Two major mechanisms have been proposed to explain the efficiency of HDL in promoting cholesterol efflux. The first pathway involves the interaction of lipid-free or lipid-poor apolipoproteins with ABCA1 (6) and the formation of new particles by cellular lipid and extracellular apolipoproteins. This process is unidirectional and requires ATP as an energy source, mediating not only the removal of FC from the plasma membrane but the mobilization of internal pools as well. In addition to the ABCA1 transporter, which is highly expressed in liver and macrophages, ABCG1 and ABCG4 mediate cholesterol transport in tissue macrophages and brain cells, respectively (6).

A second mechanism for FC removal is a nonspecific efflux from the plasma membrane by physicochemical, passive exchange between the cell membrane and extracellular acceptors. This process is favored by extracellular cholesterol esterification by LCAT, which, when activated by apoA-I, drives the mass action kinetics of the aqueous diffusion mechanism.

The importance of passive lipid removal maintaining lipid homeostasis has been addressed (7). Both diffusion-

Abbreviations: apoA-I, apolipoprotein A-I; DOPC, 1,2-dioleoyl-*sn*-glycero-3-phosphocholine; DPPC, 1,2-dipalmitoyl-*sn*-glycero-3-phosphocholine; FC, free cholesterol; FCS, fluorescence correlation spectroscopy; GP, generalized polarization; GUV, giant unilamellar vesicle; LAURDAN, 6-lauroyl-2-(dimethylamino) naphthalene;  $l_o$ ,  $l_d$ , liquid-ordered and liquid-disordered phases, respectively; M $\beta$ CD, methyl- $\beta$ -cyclodextrin; rHDL, reconstituted high density lipoprotein; SPM, porcine brain sphingomyelin.

<sup>1</sup>To whom correspondence should be addressed.  
e-mail: susanas@uci.edu

Manuscript received 18 October 2006 and in revised form 9 March 2007 and in re-revised form 30 April 2007.

Published, *JLR Papers in Press*, May 7, 2007.  
DOI 10.1194/jlr.M600457-JLR200

Copyright © 2007 by the American Society for Biochemistry and Molecular Biology, Inc.

This article is available online at <http://www.jlr.org>

mediated and scavenger receptor class B type I efflux occur to phospholipid-containing acceptors, and in contrast to the ABCA1 pathway, FC transfer is bidirectional (8). The extent and direction of the net movement depend on the ratio of efflux to influx and are determined by the properties of the acceptor and donor (9). It has been proposed that factors reducing the packing density of lipid molecules would enhance the rate of cholesterol transfer (10).

The distribution of lipids at the plasma membrane is not homogenous. It is known that cholesterol together with saturated lipids, sphingomyelin, and proteins form discrete structures called lipid rafts (11, 12), which have been associated with important biological processes such as endocytosis, adhesion, signaling, protein transport, apoptosis, and cytoskeleton organization (13). Both raft domains and the surrounding lipid matrix are liquid phases, but lipid rafts are a more organized phase (liquid-ordered) (14).

Here, we report the effect of cholesterol distribution and the lipid packing of the bilayer on the removal of the sterol by HDL particles. To facilitate the interpretation of the results, we selected well-defined model systems: reconstituted high density lipoprotein (rHDL) particles and giant unilamellar vesicles (GUVs). rHDLs, having two apoA-I molecules per particle and variable phospholipid content, are particularly useful models and are well characterized. The specie selected for this study have well-defined diameter (78 Å), a known apoA-I conformation (15), the capacity to activate LCAT (5), and binding affinity for scavenger receptor class B type I receptor (16) and POPC bilayers (17). GUVs constitute an ideal model for microscopic studies because of their size (20–50 μm); this fact permits the direct observation of micrometer-scale domains that can be observed directly by fluorescence microscopy and the study of liquid phases from a more controlled physical perspective than is possible in cells. The GUVs have been used extensively in different studies (18–23), and we have used them to study the interaction of phospholipase A<sub>2</sub> (24), apoA-I, and rHDL with lipid bilayers (17, 25, 26). We used LAURDAN generalized polarization (GP) imaging to characterize phase organization in GUVs made of different lipid mixtures containing cholesterol, and we show the usefulness of this technique to quantify the kinetics of cholesterol removal from different membrane pools.

Our previous observations in lipid-free apoA-I (25) show that the interphase in the areas where the liquid-ordered and liquid-disordered (*l<sub>o</sub>* and *l<sub>d</sub>*) phases meet facilitates the solubilization of lipids preferentially from the liquid phase of the mixture. The experiments presented here show that in the case of rHDL, phase separation is not a necessary condition for lipid (phospholipid and cholesterol) solubilization. A more important criterion is the accessibility of cholesterol defined by the particular characteristic of the lipids present at the bilayer.

## MATERIALS AND METHODS

Human apoA-I was purified from blood plasma purchased from the Champaign County Blood Bank, Regional Health Cen-

ter, as described previously (27). Porcine brain sphingomyelin (SPM), FC, and phospholipids were obtained from Avanti Polar Lipids (Alabaster, AL) and used without further purification. The phospholipids used were POPC, 1,2-dipalmitoyl-*sn*-glycero-3-phosphocholine (DPPC), and 1,2-dioleoyl-*sn*-glycero-3-phosphocholine (DOPC). Alexa 488 (Alexa Fluor, 488 carboxylic acid, succinimidyl ester) and LAURDAN were purchased from Molecular Probes (Eugene, OR). Tris (hydroxymethyl) aminomethane hydrochloride (Trizma HCl) was obtained from Sigma Biochemicals (St. Louis, MO).

### Alexa 488 labeling of apoA-I

Labeling of apoA-I with Alexa 488 was done according to published protocols (17). Briefly, apoA-I (2–4 mg) in 0.1 M sodium bicarbonate, pH 8.3, was incubated with Alexa 488 (dissolved in the same buffer) at a molar ratio 30:1 probe to protein. After 2 h of incubation in the dark at room temperature, unreacted probe was separated by elution through a NAP 5 column (Amersham Biosciences, Uppsala, Sweden), followed by overnight dialysis against 10 mM Tris, 0.15 M NaCl, 1 mM NaN<sub>3</sub>, and 0.1 mM EDTA, pH 8.0 (TBS). The efficiency of labeling of amino groups in apoA-I was determined from absorbance measurements on the conjugate at 280 nm ( $\epsilon_{280} = 57,800 \text{ M}^{-1}$  for the probe and  $30,700 \text{ M}^{-1}$  for apoA-I) and at 492 nm ( $\epsilon_{492} = 71,000 \text{ M}^{-1}$  for Alexa 488) (28). Under these conditions, approximately one molecule of probe was bound per molecule of apoA-I.

### Preparation of rHDL

rHDL particles of 78 Å diameter were prepared by the sodium cholate dialysis method (29), using a starting molar ratio of POPC/protein/sodium cholate of 35:1:60. The desired amount of POPC in CHCl<sub>3</sub> was dried under N<sub>2</sub>, and the lipids were dispersed in TBS; sodium cholate was added, and the mixture was kept at 37°C until the lipid dispersion cleared. Next, the mixed micelles were incubated in the presence of the proteins for 1 h at 37°C and dialyzed extensively against TBS at 4°C. The homogeneity and hydrodynamic diameter of the rHDLs were estimated by native (8–25%) polyacrylamide gradient gel electrophoresis on a Pharmacia Phast System. Protein was quantified either by absorbance at 280 nm or with the Bio-Rad Protein Assay (Bio-Rad, Hercules, CA). When necessary, preparations were passed through a Superdex 200 HR 10/30 column (Pharmacia FPLC System) equilibrated with the same buffer at a flow rate of 0.25 ml/min. Fractions that were free of higher molecular weight complexes after the first column elution were concentrated and further purified by a second chromatographic step. For this step, the same column was equilibrated with TBS plus 0.1 M guanidine hydrochloride, and a flow rate of 0.4 ml/min was used. After the elution, pure fractions were dialyzed against TBS.

### GUV formation

The protocol to form GUVs is a modified version of the method published by Angelova and colleagues (18, 19). Briefly, stock solutions of phospholipids were prepared in chloroform at a concentration of 0.2 mg/ml. Two microliters of the stock was added to each platinum wire of the growing chamber and dried under N<sub>2</sub> for ~30 min to remove any traces of the remaining solvent. The chamber was sealed with a cover slip and thermostatted with a water-circulating bath at the growing temperature (normally 10°C over the corresponding transition temperature of the lipid). Immediately before connecting the platinum wires to the function generator (Hewlett-Packard, Santa Clara, CA), 1 mM Tris buffer, pH 8.0 (previously warmed up to the growing temperature), was added to the chamber. Temperature was monitored by a digital thermocouple (model 400B; Omega, Stamford,

CT) in contact with the wires. A low-frequency alternating current field (frequency, 10 Hz; amplitude, 2 V) was applied to the platinum wires to grow the vesicles by the electroformation method. A charge-coupled device color video camera (CCD-Iris; Sony) attached to the microscope allowed visualization of vesicle formation and selection of the target GUVs.

### GP image measurements

**LAURDAN GP.** LAURDAN is used as a membrane probe because of its large excited-state dipole moment, which results in its ability to report the extent of water penetration into the bilayer surface as a result of the dipolar relaxation effect (30). Water penetration has been correlated with lipid packing and membrane fluidity (31, 32). The emission spectrum of LAURDAN in a single phospholipid bilayer is centered at 440 nm when the membrane is in the gel phase and at 490 nm when it is in the liquid crystalline phase. The GP gives a mathematically convenient and quantitative way to measure the emission shift. The function is given by:

$$GP = \frac{I_{440} - I_{490}}{I_{440} + I_{490}} \quad (1)$$

where  $I_{440}$  and  $I_{490}$  are the emission intensities at 440 and 490 nm, respectively. A full discussion of the use and mathematical significance of GP can be found in the literature (32, 33). If LAURDAN is solubilized in a lipidic structure, such as a liposome, its spectrum will move according to the water content of the bilayer. The fluorescence emission of LAURDAN at the liquid-ordered bilayer is blue-shifted, compared with the emission from the liquid-disordered bilayer, allowing identification of the phase of the lipid domain directly from the GP image. To calculate the GP value in a two-photon microscope, an excitation wavelength of 780 nm and a two-channel system with the corresponding filters on the emission are used (see below for details).

**Experimental setup.** Images were collected on a scanning two-photon fluorescence microscope designed at the Laboratory for Fluorescence Dynamics (University of Illinois at Urbana-Champaign, Urbana, IL) (34, 35). A LD-Achroplan 20× long-working-distance air objective with a numerical aperture of 0.4 (Zeiss, Holmdale, NJ) was used. A mode-locked titanium-sapphire laser (Mira 900; Coherent, Palo Alto, CA) pumped by a frequency-doubled Nd:vanadate laser (Verdi; Coherent) and set to 780 nm was used as the two-photon excitation light source. A galvanometer-driven  $x$ - $y$  scanner was positioned in the excitation path (Cambridge Technology, Watertown, MA) to achieve beam scanning in both the  $x$  and  $y$  directions. Samples received from 5 to 9 mW of 780 nm excitation light, and a frame rate of 9 frames/s was used to acquire the 256 × 256 pixel images. A quarter wave-plate (CVI Laser Corp., Albuquerque, NM) was aligned and placed in the path of the beam before the light entered the microscope to minimize the polarization effects of the excitation light. Fluorescence emission was observed through a broad band-pass filter from 350 to 600 nm (BG39 filter; Chroma Technology, Brattleboro, VT). A miniature photomultiplier (R5600-P; Hamamatsu, Bridgewater, NJ) was used for light detection in the photon-counting mode, and counts were acquired using an ISS card (ISS, Inc., Champaign, IL).

A two-channel detection system was attached for GP image collection. The fluorescence was split into red and blue channels using a Chroma Technology 470DCXR-BS dichroic beam splitter in the emission path. Interference filters (Ealing 490 and Ealing 440) were placed in the emission paths to further isolate the red and blue parts of the emission spectrum. Separate detectors were used for each channel to simultaneously collect 490 and 440 nm

emission. Red and blue images were collected simultaneously and then recombined to form the GP image of the sample using the SimFCS program (Laboratory for Fluorescence Dynamics). Corrections for the wavelength dependence of the emission detection system were accomplished through the comparison of the GP value of a known solution (LAURDAN in DMSO) (21, 36) taken on an ISS Inc. model PC1 steady-state fluorometer and then in the microscope.

**GP data analysis.** Two simultaneous 256 × 256 pixel images are obtained from the vesicle (image channel 1 and image channel 2), which are processed applying the GP formula (equation 1) to each pixel of the image using the SimFCS program. The resulting image (GP image) can be represented in a histogram of the number of pixels with a given GP. The center of the histogram represents the average GP. GP values can range from -1 to +1 according to equation 1, and a color scale is used to visualize pixels with different GP values.

When the mixture presents areas with different GP values, both the histogram and the GP image can be deconvoluted into higher and lower GP values, and then the average GP will be given by

$$GP_{avg} = GP_1xf_1 + GP_2xf_2 \quad (2)$$

where  $f_1$  and  $f_2$  correspond to the fractional contributions of the components with higher ( $GP_1$ ) and lower ( $GP_2$ ) GP values.

**GP kinetics measurements.** GUVs were grown as explained previously at 60°C in 1 mM Tris, pH 8.0. Temperature was monitored continuously using a thermocouple attached to the platinum wires. For GP measurements, LAURDAN in DMSO was added to the GUVs (in a 1:300 LAURDAN/lipid molar ratio) and incubated for 15 min. For the kinetics experiments, the temperature was decreased to the desired value and the time zero GP image was taken. To ensure quick mixing, cholesterol acceptors [apoA-I, rHDL, and methyl- $\beta$ -cyclodextrin (M $\beta$ CD)] were previously diluted in the growing buffer and then added to the chamber. For most of the experiments, the final concentration of apoA-I or rHDL in the solution was 0.35  $\mu$ M  $\mu$ g/ml (expressed as protein concentration). After addition of the acceptors, GP images were taken every 15 min for 2 h. To prevent morphological changes in the GUV attributable to osmotic differences, dextrans were prepared in 1 mM Tris, pH 8.0, and particles and apoA-I were dialyzed overnight against the same buffer.

### Fluorescence correlation spectroscopy measurements

**Fluorescence correlation spectroscopy.** Fluorescence correlation spectroscopy (FCS) is widely used and well-described in numerous reports (37–41). Briefly, FCS measures the fluctuations in fluorescence produced when the fluorescent molecules move through the illuminated volume. The analysis of these types of fluctuations can be done with the autocorrelation or with the photon-counting histogram method. The autocorrelation function,  $G(\tau)$ , characterizes the time-dependent decay of the fluorescence fluctuations to their equilibrium value. From the autocorrelation function, one can recover two parameters: the diffusion coefficient and the average number of particles in the observation volume ( $N$ ), which is given by the inverse of  $G(0)$ . In the photon-counting histogram approach, the probability of detecting a given number of photons per sampling time is determined. This probability is experimentally determined using a histogram of the photons detected per bin time. Two parameters will characterize the photon distribution: the number of molecules in the observation volume ( $N$ ) and the molecular brightness ( $\beta$ ), defined as the average number of photons detected per sampling time per second (42).



**Microscope setup.** For FCS measurements, a microscope setup similar to that used for the GP measurements was used. The differences were as follows: *i*) the excitation light source for 780 nm was a mode-locked titanium-sapphire laser with 80 MHz, 100 fs pulse width (Tsunami; Spectra-Physics, Mountain View, CA); *ii*) a one-channel setup with a photomultiplier tube (Hamamatsu R7400P) was used for light detection in the photon-counting mode; and *iii*) a BG39 optical filter (Chroma Technology) was placed before the photomultiplier for the suppression of infrared excitation light. A Zeiss C-Apo 40 $\times$  (1.2 numerical aperture) water-immersion objective lens was used for the measurement.

**FCS kinetics measurements.** POPC/FC (2:1 molar ratio) GUVs were grown at 25 $^{\circ}$ C in 2 ml of 1 mM Tris, pH 8.0. Alexa 488-labeled rHDLs were added to the growing chamber as explained above. The system was thermostatted using a water bath, and the temperature was monitored with a thermocouple attached to the platinum wires. Every 15 min for 2 h, an image of the GUV was taken and the laser was directed to a point just outside the GUV to perform the FCS measurement.

**FCS data analysis.** Experimental autocorrelation functions were fit using a Gaussian-Lorentzian intensity profile model, as described previously (24, 37), which contains the formulas for the point-spread function and the definition of the beam waist used. The beam waist of the excitation profile function depends on the instrument setup and must be calibrated each time the system is aligned; for this purpose, fluorescein was used. In 25 mM Tris buffer (pH 8.0) at 25 $^{\circ}$ C, fluorescein has a diffusion coefficient of 300  $\mu\text{m}^2/\text{s}$  (38). The recovered beam waist value of 0.41  $\mu\text{m}$  was used to perform the autocorrelation analysis and determine the diffusion coefficient of the Alexa 488-labeled rHDL particles during their interaction with the GUVs. Photon-counting analysis was also done to determine the molecular brightness and the particle number of the labeled rHDL particles during the kinetics, assuming a Gaussian-Lorentzian intensity profile. Both types of analysis were performed using the program SimFCS (Laboratory for Fluorescence Dynamics).

## RESULTS

### Changes in GP are attributable to changes in cholesterol content

GUVs made of POPC plus different amounts of cholesterol were grown in independent chambers, incubated with LAURDAN, and the GP images of 10 GUVs were taken and averaged. The point-spread function of the two-photon excitation defines an illumination volume close to a 1 fL with a geometry that gives a distance in Z plane of  $\sim 1$ –1.5  $\mu\text{m}$ . Therefore, a 1  $\mu\text{m}$  slice taken at the center of the spherical liposome will appear as a fluorescent ring corresponding to LAURDAN emission within the phospholipid bilayer with a black nonfluorescent central area (LAURDAN does not fluoresce in water).

Figure 1A shows the plot of GP as a function of cholesterol content. As cholesterol concentration increases, GP increases at 25 $^{\circ}$ C and 37 $^{\circ}$ C in a linear trend until 45 mol%. To correlate the changes in GP value and the cholesterol content in the bilayer, GUVs containing cholesterol were incubated with increasing concentrations of a well-known cholesterol acceptor, M $\beta$ CD (23, 43, 44). Figure 1B shows the dependence of the GP on the M $\beta$ CD concentration at 25 $^{\circ}$ C. A linear trend was observed until 800  $\mu\text{M}$  M $\beta$ CD. A linear dependence in the same concentration range was also observed at 37 $^{\circ}$ C (data not shown). This last concentration was enough to decrease the GP to the value measured in GUVs containing only POPC. At dextrin concentrations > 800  $\mu\text{M}$ , the GUVs shrank.

### Cholesterol removal by rHDL

rHDLs are also known as cholesterol acceptors. Figure 1C shows that GP in POPC/FC (2:1) GUVs decreases in a linear manner when incubated for 2 h with increasing concentrations of 78  $\text{\AA}$  rHDL at 25 $^{\circ}$ C. This trend is ob-

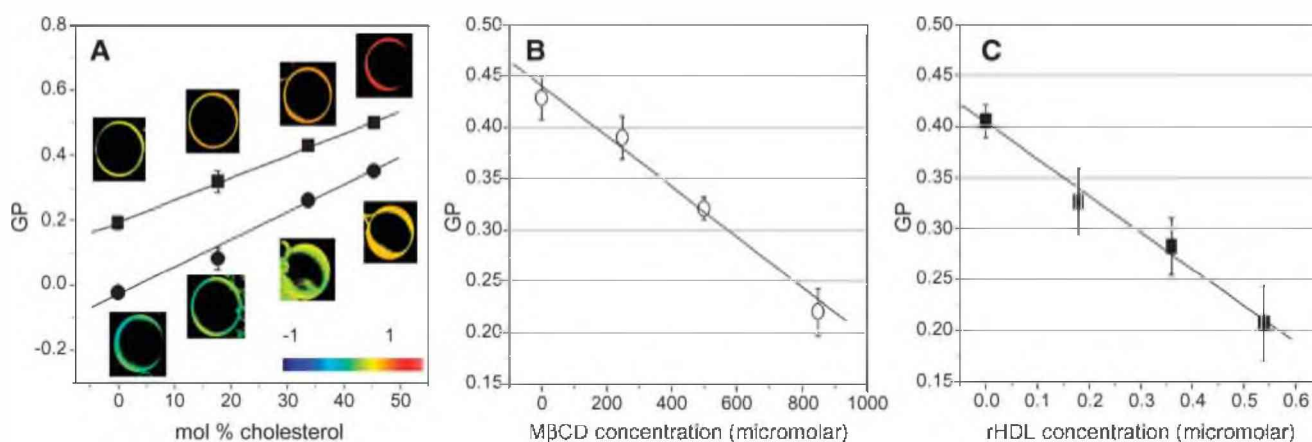


**Fig. 1.** Generalized polarization (GP) changes as a function of cholesterol content. A: Giant unilamellar vesicles (GUVs) made of POPC plus different percentages of cholesterol were grown at 25 $^{\circ}$ C (squares) and 37 $^{\circ}$ C (circles). Independent chambers were prepared for each cholesterol concentration. Lines correspond to the linear fit of the experimental data at 25 $^{\circ}$ C [ $\text{GP} = 0.197 + 0.679 \times 10^{-2} \times \% \text{ free cholesterol (FC)}$ ] and at 37 $^{\circ}$ C [ $\text{GP} = -0.026 + 0.846 \times 10^{-2} \times \% \text{ FC}$ ], and images show an example of a GUV at each cholesterol concentration using the same scale and color code. B, C: Different concentrations of methyl- $\beta$ -cyclodextrin (M $\beta$ CD) (B) and reconstituted particles of 78  $\text{\AA}$  diameter (C) were added to POPC/FC (2:1) GUVs at 25 $^{\circ}$ C and incubated for 2 h. Average GP values of 10 GUVs and SD are shown. rHDL, reconstituted high density lipoprotein.

served in the range 0–0.56  $\mu\text{M}$  (calculated as protein concentration), a concentration range 1,000 times lower than that required for M $\beta$ CD to achieve the same GP changes.

The time courses of the GP changes when POPC/FC GUVs are incubated with 0.35  $\mu\text{M}$  rHDL at 25°C and 37°C are shown in Fig. 2. At 25°C, the GP decreases from 0.39 to 0.26, and at 37°C, it decreases from 0.25 to 0.12. The data from Fig. 1A can be used to calculate the amount of cholesterol removed from the bilayer. After 2 h, similar amounts of cholesterol are removed at both temperatures ( $19.4 \pm 0.5\%$  at 25°C and  $14.1 \pm 0.3\%$  at 37°C); however, the process is faster at 37°C (half-time of  $48.1 \pm 0.9$  min) than at 25°C (half-time  $59.6 \pm 0.2$  min).

Control experiments, described below, were done to show that changes in GP observed in the presence of rHDL were attributable to changes in the concentration of cholesterol on the bilayer and not to other factors.

i) During the interaction of rHDL and the GUV, LAURDAN from the GUV may transfer to the particle. If rHDLs containing LAURDAN bind the bilayer, the GP value measured (on the bilayer) would have the contribution of the intensity coming from the LAURDAN molecules solubilized both at the GUVs and in the rHDLs (equation 2). In a standard kinetic experiment, the total intensity from the target GUV labeled at a LAURDAN/lipid ratio of 1:300 is 60,000 counts on average per channel. A 0.35  $\mu\text{M}$  solution of rHDL (the concentration used in all experiments) labeled at a LAURDAN/lipid ratio of 1:300 shows  $\sim 200$  counts on average (i.e., on the order of background noise). Thus, because of their low concentration, the intensity contribution of the LAURDAN in the rHDL to the total GP value measured in the GUV will be negligible, and no changes in the GP of the bilayer can be attributed to the LAURDAN in the rHDL. Binding of the

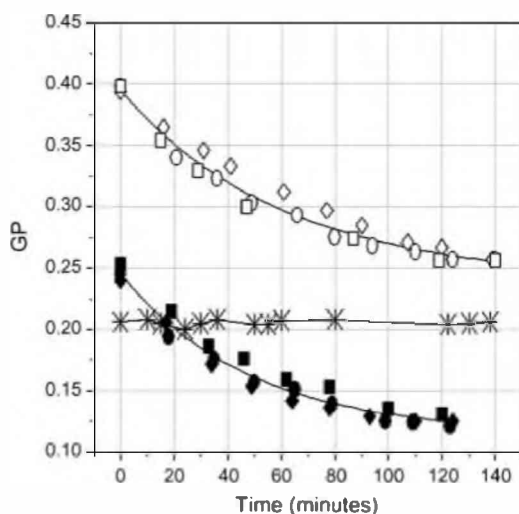


**Fig. 2.** Changes in 6-lauroyl-2-(dimethylamino) naphthalene (LAURDAN) GP of POPC (asterisks) and POPC/FC (2:1) GUVs (symbols) after the addition of 0.35  $\mu\text{M}$  78 Å rHDL. Different symbols (squares, circles, and diamonds) correspond to three sets of experimental data at 25°C (open symbols) and 37°C (closed symbols). Solid lines correspond to the first-order exponential decay fitting for the average of the three experimental data sets.

particles to the POPC/FC GUVs was tested using rHDLs containing Alexa 488-labeled apoA-I (17) at the same concentration used in all experiments (0.35  $\mu\text{M}$ ), and no binding was detected during 2 h of incubation. In addition, we previously observed that under the same experimental conditions, 78 Å rHDLs bind to pure POPC GUVs (17), and we show here that this binding did not change the GP of the bilayers in a 2 h period (Fig. 2). These results indicate that even if rHDLs bind to the membrane, the GP of the GUV will not be modified.

ii) To achieve net zero cholesterol efflux, GUVs made of POPC/FC (2:1) were incubated with 0.35  $\mu\text{M}$  rHDL containing the same POPC/FC ratio. No changes in GP value were observed during the 2 h observation period.

iii) Finally, as a negative control, we used lipid-free apoA-I. The lipid-free protein is known to require the presence of the ABCA1 transporter to remove FC; therefore, it is not expected to show significant cholesterol removal from artificial membranes. Incubation of POPC/FC GUVs with 0.35  $\mu\text{M}$  apoA-I did not change the GP values after the 2 h incubation (data not shown).

### rHDL during cholesterol removal

To study the behavior of 78 Å rHDL during cholesterol removal, we used FCS. In Fig. 3A, we show an intensity image of an unlabeled POPC/FC GUV after 2 h of incubation with Alexa 488 rHDL. The laser beam was localized in the solution close to the bilayer, and FCS measurements were performed at different times. Time zero corresponds to a measurement taken immediately after the addition of the labeled particle to the solution. Figure 3B shows the changes in diffusion coefficient of the 78 Å rHDL particles during the incubation period.

The theoretical diffusion coefficient of a molecule can be calculated using the Stokes-Einstein equation (39); in the case of 78 Å rHDL with a molecular mass of  $\sim 70,000$  Da, this value is  $\sim 51 \mu\text{m}^2/\text{s}$ . The experimental diffusion coefficient calculated from the autocorrelation analysis at time zero is  $48 \pm 3 \mu\text{m}^2/\text{s}$  and decreases with the incubation time to  $32 \pm 4 \mu\text{m}^2/\text{s}$  (Fig. 3B). The photon-counting histogram analysis (Fig. 3C) indicates that the brightness of the molecules does not change during the 2 h experiment. These results imply that the aggregation state of the molecule does not change and the process of cholesterol removal is carried out by individual rHDL particles, which increase in size during the interaction.

### Distribution of cholesterol at the bilayer

To analyze the influence of lateral phase organization on lipid removal, we first characterized GUVs made of two raft-like mixtures: DOPC/DPPC/FC (1:1:1) and POPC/SPM/FC (6:1:1). We chose DOPC for the first ternary mixture because this mixture is already well characterized in the literature (45). Figure 4A shows the GP values versus temperature for the DOPC/DPPC/FC mixture. Above 32°C, the GP image is homogeneous and one GP value is obtained (image at 36°C in Fig. 4A), as is the case for POPC/FC (Fig. 1A). Below 32°C, a clear separation of two

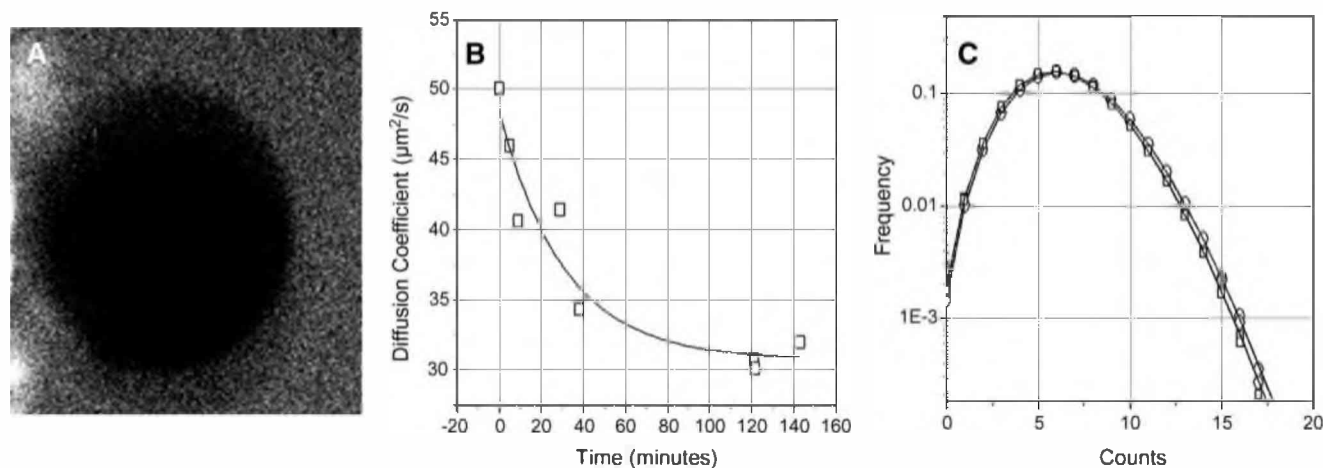


**Fig. 3.** Interaction of 78 Å rHDL with POPC/FC (2:1) GUVs followed by fluorescence correlation spectroscopy (FCS). A: Fluorescence image of an unlabeled POPC/FC GUV after 2 h of incubation with 0.35 µM Alexa 488-labeled 78 Å rHDL. B: Diffusion coefficient obtained from the autocorrelation analysis of FCS data taken during a 2 h period in the solution outside the GUV close to the membrane. The experimental data fitted to a one-exponent decay with a time constant of  $30.7 \pm 11$  min. C: Photon-counting histogram analysis of the first (squares) and last (circles) records from the kinetics shown in B. In B and C, symbols correspond to the experimental data and the line corresponds to the best fit.

macroscopic phases occurs (image at 25°C in Fig. 4A) and two GP values can be calculated, as explained in Methods and reported for each temperature. Phase separation is observed in 100% of the vesicles in the chamber for all of the experiments performed, and after a short time at this temperature, domains do not move significantly. Control experiments show constant GP values and areas for both phases during a 2 h period, indicating that the reported changes in the area and the GP cannot be attributed to small movements of the entire GUV and/or the domains (data not shown). The image at 27°C (inserted in the plot of Fig. 4A) shows the GUV structure at the transition before total phase separation occurs; this structure lasts a few minutes and can be observed if the temperature is decreased slowly. This image shows small “islands” of higher GP (0.495) appearing as “floating” in a matrix of lower GP (0.299).

In the case of the POPC/SPM/FC mixture, above 30°C only one phase is observed (Fig. 4B) and the average GP is constant over the entire GUV. Below 30°C, a clear separation of two macroscopic phases occurs and two GP values are calculated for each temperature. These GUVs are extremely heterogeneous in size, and ~60% of the vesicles in the chamber exhibit phase separation. The observed high-GP domains are small (probably one-sixth to one-tenth of the low-GP domains) and vary in size among GUVs in the same chamber and between experiments. The results described below pertain to those vesicles in which larger domains were found.

To study the interaction of the rHDL particles with the two raft-like mixtures, two temperatures were chosen: one above the transition temperature, at which one homogeneous phase can be observed, and a second below the transition temperature, at which two liquid phases coexist (12, 45).

#### Interaction of rHDL with DOPC/DPPC/FC (1:1:1)

With the purpose of predicting the direction of the changes in GP value when cholesterol is removed from DOPC/DPPC/FC, we compared this mixture with DOPC/DPPC. The GP-versus-temperature plot for the two mixtures is shown in Fig. 5A and repeated in Fig. 5C for comparison purposes. At 60°C, both mixtures present a homogeneous phase and one GP value is reported. Below 45°C (for the binary mixture) and <36°C (for the ternary mixture), phase separation is observed and two GP values are reported.

Figure 5A shows the comparison of the two mixtures at 36°C. At this temperature (solid vertical line), the mixture containing cholesterol presents one homogeneous phase and therefore one GP value (intersection of the temperature line and the closed circles curve), whereas the same mixture without cholesterol shows domain coexistence and their respective GP values are shown by the intersection of the solid line with the open circles curve. Thus, the expected changes if cholesterol is removed under these conditions are a phase separation and the corresponding change from one to two GP values, in the direction indicated by the arrows. Figure 5B shows the time-dependent GP changes after the addition of 0.35 µM 78 Å rHDL [a concentration that was effective for removing cholesterol from POPC/FC GUVs (Fig. 2)]. No changes in GP value were observed in a 2 h period, indicating that no cholesterol is being removed. Instead, incubation with 0.25 mM MβCD induced a GP change from 0.37 to 0.15 (Fig. 5B, diamonds), but no phase separation was observed. This last observation might be attributable to the lower concentration of MβCD used in this study compared with previously reports, in which phase separation was observed (46).

In a similar manner, Fig. 5C shows the expected GP changes if cholesterol is removed from a DOPC/DPPC/



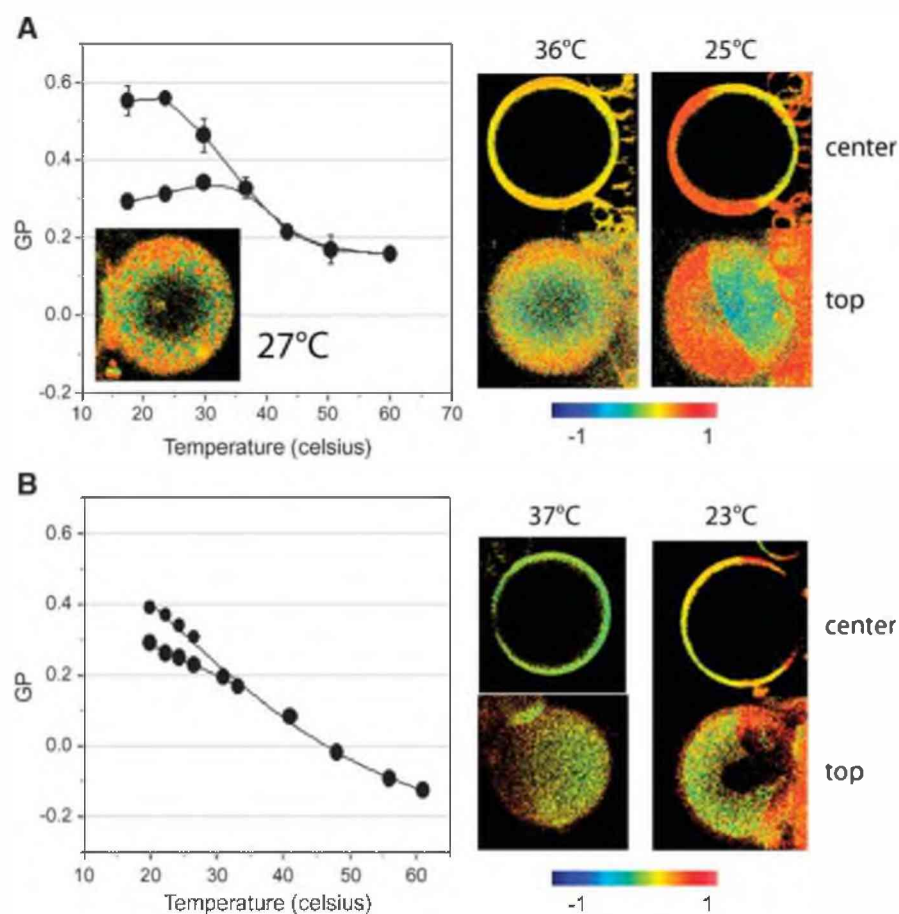


**Fig. 4.** Changes in GP as a function of the temperature of DOPC/DPPC/FC (1:1:1) (A) and POPC/SPM/FC (6:1:1) (B). Symbols correspond to the average GP of 10 independent GUVs. Above phase separation, one average GP is presented; below transition temperature, two phases coexist and two GP values are plotted for each temperature. GP images at right show the center and top views of a GUV at the working temperature for each mixture. Panel A also shows the top view of a DOPC/DPPC/FC (1:1:1) GUV at 27°C.

FC (1:1:1) mixture at 25°C. At this temperature, both mixtures (with and without cholesterol) show phase separation. The expected changes if cholesterol is removed are an increase in the GP value of the higher GP phase and a decrease of the GP of the lower GP phase. Figure 5D shows the time-dependent changes of the GP value for both phases after the addition of 0.35  $\mu\text{M}$  78 Å rHDL. The GP value of the higher GP phase (circles) did not change significantly, similar to the results at 36°C. However, the GP value of the lower GP phase (squares) did show a decrease during the incubation. This observation suggests a preferential cholesterol removal from the lower GP phase by rHDL. No significant changes in the area of the coexisting phases or the size of the GUV were observed.

#### Interaction of rHDL with POPC/SPM/FC (6:1:1)

Using a similar rationale, we analyzed the influence of phase separation on cholesterol removal from POPC/SPM/FC (6:1:1) GUVs. At 37°C, the intersection of the solid line with the GP curves in **Fig. 6A** indicates that a decrease in GP (from the closed circle curve toward the open circle curve) without phase separation is expected if cholesterol is removed. Experimental data from after

the addition of 0.35  $\mu\text{M}$  78 Å rHDL show no significant changes during the observed period of 2 h (squares in **Fig. 6B**), indicating, similar to the POPC/DPPC/FC mixture at 36°C (**Fig. 5B**), that no cholesterol is being extracted.

At 23°C, the expected result if cholesterol is removed from the GUV is a decrease in the GP value in both coexisting phases (**Fig. 6C**). In agreement with the observations using the previous mixture, a decrease in GP value is observed in the lower GP phase (blue circles in **Fig. 6D**) but not in the higher GP domains (orange squares in **Fig. 6D**). This result indicates that also for this mixture, rHDL preferentially removes cholesterol from the lower GP phase.

During the interaction, the higher GP domains tended to move, making the quantification of the areas difficult; however, it was observed that a clear decrease in size (area) of these domains was sometimes accompanied by a decrease in the overall size of the GUVs (**Fig. 6D**).

## DISCUSSION

In this work, we used an original experimental design to demonstrate that cholesterol removal by rHDL depends

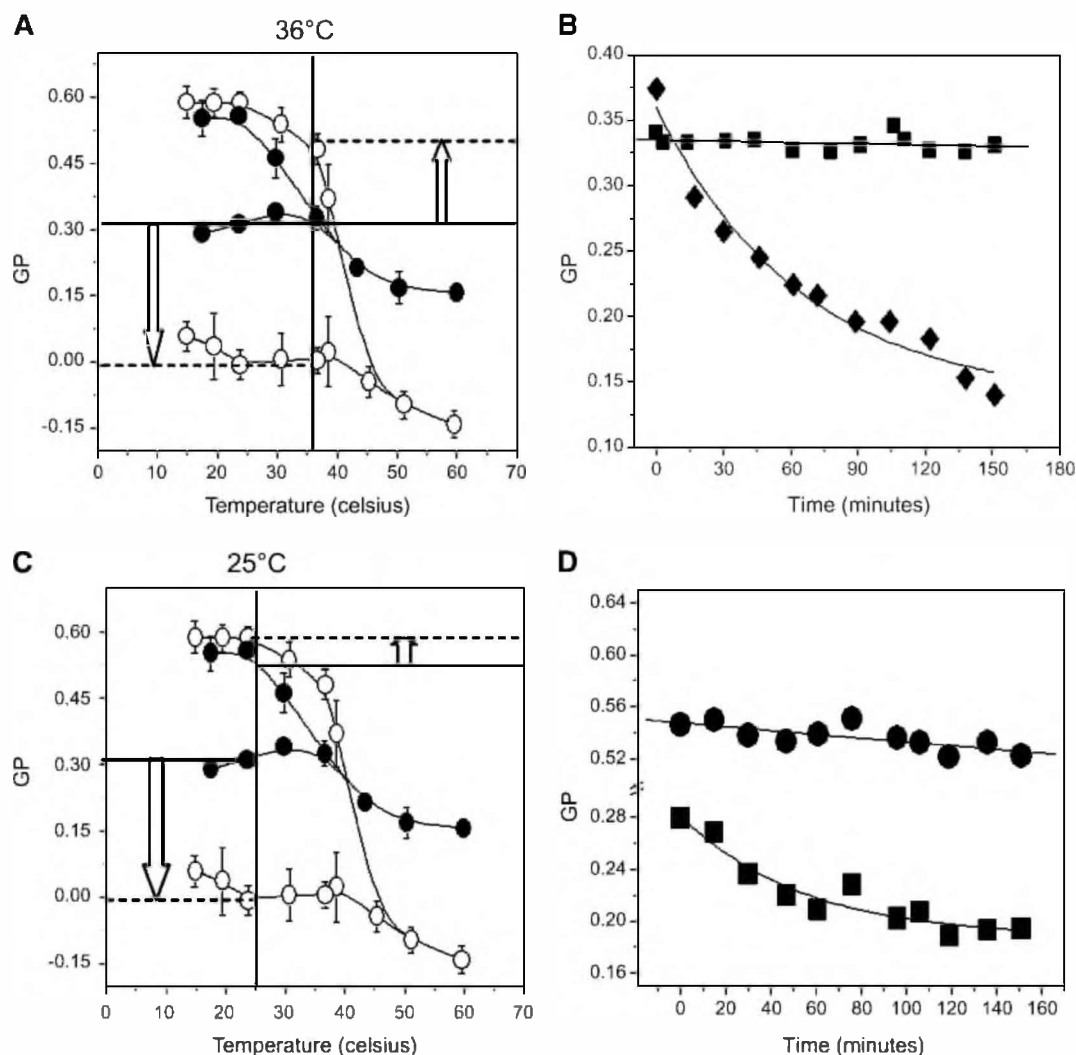


**Fig. 5.** DOPC/DPPC/FC (1:1:1) GUVs plus cholesterol acceptors. Expected GP changes (A, C) and kinetics (B, D) for cholesterol removal at 36°C (upper panels) and 25°C (lower panels). A, C: GP values at each temperature are shown with closed or open circles for GUVs containing or not containing FC, respectively. If FC is removed at the temperatures indicated by the solid vertical lines, GP is expected to change from the initial values (closed circles) in the direction shown by the white arrows toward the GP values with no FC (open circles). B: GP changes after the addition of 0.35  $\mu\text{M}$  78 Å rHDL (squares) and 0.25 mM M $\beta$ CD (diamonds) to DOPC/DPPC/FC (1:1:1) GUVs at 36°C. Lines represent the linear square fit of the experimental data. D: GP changes after the addition of 0.35  $\mu\text{M}$  78 Å rHDL to DOPC/DPPC/FC (1:1:1) GUVs at 25°C. GP kinetics for the liquid-ordered ( $l_o$ ) phase (circles) and the liquid-disordered ( $l_d$ ) phase (squares) are shown separately.

on lipid phase fluidity. We have previously shown that LAURDAN GP imaging with two-photon excitation and a dual-channel microscope offers a well-suited methodology to study lipid-protein interaction with high spatial resolution (25, 36). Here, we show the usefulness of this technique to quantify the kinetics of cholesterol removal from different membrane pools simultaneously.

First, we set out to establish the feasibility of our technique. Experiments with homogeneous liquid POPC/FC bilayers (Fig. 1) show that GP measurements are sensitive to changes in cholesterol content in the membrane according to a linear relationship up to a cholesterol concentration of 45%. Although previous work by Parasassi et al. (44, 45) shows that some discontinuities in the linear behavior could be present, differences in technical conditions could explain this apparent discrepancy.

Second, we showed the correlation between changes in GP values at the bilayer and the concentration of the cholesterol acceptor used in this work, M $\beta$ CD, and rHDL. Finally, we set out to characterize the lipid packing of the mixtures used and their behavior under cholesterol depletion. We used three well-characterized model systems: one binary mixture (POPC/FC) and two ternary raft-like mixtures, DOPC/DPPC/FC (1:1:1) and POPC/SPM/FC (6:1:1).

The phase diagram for POPC plus different cholesterol concentrations has been described (47). One feature of this phase diagram is the observation over a wide temperature range of a fluid but highly ordered phase ( $l_o$ ) at bilayers with cholesterol concentrations > 25 mol% (as we used here). This  $l_o$  phase has universal characteristics that are relatively independent of the precise chemical structure of the phosphocholine molecule.



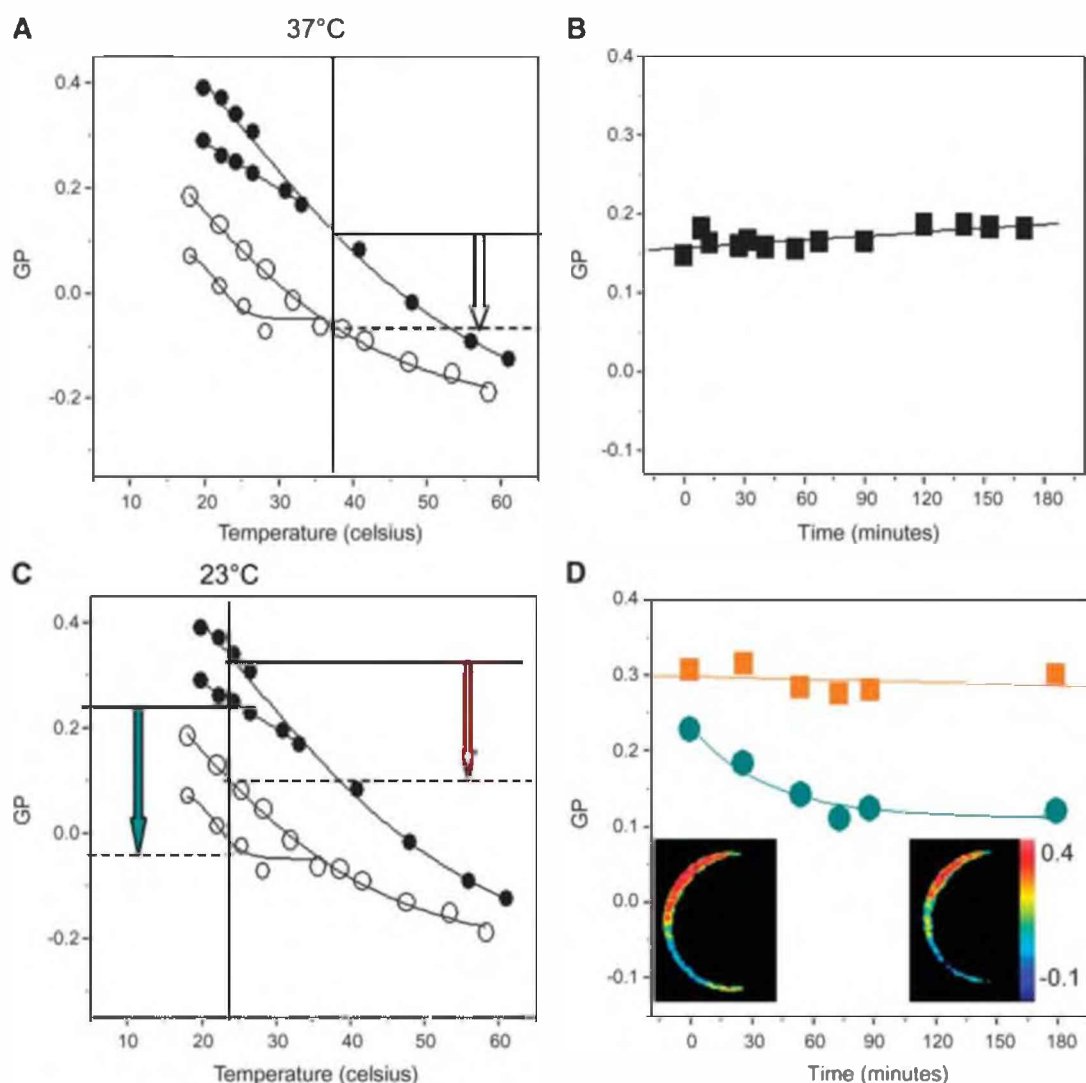


**Fig. 6.** POPC/SPM/FC (6:1:1) GUVs plus 78 Å rHDL particles at 23°C and 37°C. Expected GP changes (A, C) and kinetics (B, D) for cholesterol removal at 37°C (upper panels) and 23°C (lower panels). A, C: GP values at each temperature are shown with closed or open circles for GUVs containing or not containing FC, respectively. If FC is removed at the temperatures indicated by the solid vertical lines, GP is expected to change from the initial values (closed circles) in the direction shown by the arrows toward the GP values with no FC (open circles). B, D: Kinetics data taken after the addition of 0.35  $\mu$ M 78 Å rHDL to POPC/SPM/FC (6:1:1) at 23°C and 37°C. GP values for  $l_o$  (orange) and  $l_d$  (blue) are shown separately. Lines represent the linear square fit of the experimental data. Images correspond to the GUV in the beginning (left) and at the end (right) of the incubation period.

The phase diagram for the two raft-like lipid compositions is also available, and depending on the temperature, they present one  $l_d$  phase or a  $l_o/l_d$  phase coexistence (12, 22, 45, 48, 49). The DOPC/DPPC/FC (1:1:1) mixture has been characterized by Veatch et al. (45). In our study, this mixture presents a phase separation at  $33 \pm 1^\circ\text{C}$ . Above this value, one homogeneous GP characterizes the sample. Below this value, two phases with different GP coexist. All of these observations are in agreement with the studies done by Veatch et al. (45), who reported a transition between a homogeneous  $l_o$  phase and a coexistence of  $l_o/l_d$  phases at  $32^\circ\text{C}$ .

The second raft-like mixture was POPC/SPM/FC at a molar ratio of 6:1:1. The phase diagram at the two working temperatures has been reported by de Almeida, Fedorov, and Prieto (48), and the mixture presents  $l_o/l_d$  phase co-

existence at 23°C and a homogeneous  $l_d$  phase at 37°C. Our GP images in Fig. 4A show the homogeneous phase at 37°C and the phase separation at 23°C, in agreement with the data of Almeida, Fedorov, and Prieto (48).

#### The importance of cholesterol packing for rHDL-mediated lipid solubilization

Rothblat et al. (50) proposed that lipid packing may define several pools in the membrane, from which cholesterol can be removed with different kinetic properties. NMR studies reported that cholesterol desorption may be facilitated from phases in which interactions of phospholipids and cholesterol are weak (45). Our data support this view and show in real time that lipid packing determines the

kinetic properties of cholesterol removal. We show that rHDLs solubilize cholesterol from POPC/FC GUVs at 25 °C and 37 °C and from  $l_d$  domains coexisting with the  $l_o$  phase, but not from homogeneous  $l_d$  phases of the same mixture.

To explain our results, we looked at the molecular interactions between lipids and cholesterol in the different phases. The coexisting  $l_d$  phases are enriched in the unsaturated phospholipid (DOPC or POPC), but they also contain a percentage of the saturated lipid (DPPC or SPM) (45, 51). Clearly, the presence of small amounts of DPPC or SPM is not an impediment to the free diffusion of cholesterol to the rHDL. The unsaturations present in the acyl chains of POPC or DOPC introduce kinks that limit the ability of cholesterol to order, to mix homogeneously, to reduce interfacial elasticity (52), and to decrease in-plane elasticity (51). Thus, kinks in the lipids forming the  $l_d$  phases (DOPC and POPC) will prevent the deep penetration that is possible with the rigid acyl chains of DPPC and SPM. Cholesterol will thus locate more superficially and will more easily desorb from the membrane to the aqueous interface and transfer to the rHDL. Similar reasoning can be applied to the cholesterol present in the universal  $l_o$  phase described for POPC/FC (2:1) (47), from which the rHDL removes cholesterol as well.

On the other side, the coexisting  $l_o$  phases are formed mainly by DPPC or SPM and contain a small percentage of unsaturated lipid DOPC or POPC. DPPC has a chain structural motif more similar to natural sphingolipids than to naturally predominant phosphocholines, which are unsaturated (52).  $^2\text{H-NMR}$  data suggest that the hydrophobic thickness of the lipid bilayer is much larger than the 20 Å of the cholesterol molecule and that the average acyl chain length, in each leaflet, is significantly shorter than the length of cholesterol (53). Thus, cholesterol molecules locate part of their tail in the adjacent bilayer (54), allowing the formation of tail-to-tail dimers (55) and then impeding its desorption.

When ternary mixtures are at 37 °C, one homogeneous  $l_d$  phase exists from which particles are not able to remove cholesterol. Compared with the coexisting  $l_d$  phase, this homogeneous  $l_d$  phase contains more DPPC or SPM, which makes cholesterol nonaccessible to the rHDL and thus the kinetics of transfer much slower.

The observation that M $\beta$ CD was able to remove cholesterol from GUVs at 37 °C, whereas rHDL could not, may have an explanation in the different mechanisms for cholesterol removal used by these particles. It has been postulated that cholesterol has to desorb completely from the plasma membrane into the aqueous medium before it can be absorbed by the rHDL (8). In contrast, the M $\beta$ CD mechanism appears to involve the direct incorporation of cholesterol into the hydrophobic cavity of the cyclodextrin molecule, without the necessity of its traveling through an intermediate aqueous phase (56–58).

### Importance of the acceptor

Even though rHDLs have been used extensively as a model system in studies referring to cholesterol removal

(16, 17), not much attention has been focused on the particle itself. We show here that the acceptance of cholesterol by rHDL modifies its diffusion (i.e., its size). The FCS data taken outside the GUV membrane indicate that rHDLs act as independent units in the process of cholesterol removal. The lipid molecules are incorporated into the particle, and the consequent increase in size is evident in a decrease in lateral mobility observed. It is possible that during the interaction of the particles with the bilayer, some phospholipids are removed in addition to cholesterol. We have shown this previously by analyzing the rearrangement of 78 Å rHDLs during the interaction with phospholipid vesicles (17). These observations are important, as apoA-I conformation is strongly dependent on particle size (59), and its interaction with membranes, as well as its lipid diffusion mechanism, must change upon lipid enrichment. Although rHDLs are more lipidated than natural pre $\beta$ -HDLs isolated from human plasma, these observations support our previous hypothesis that the metabolic dynamics of discoidal lipid-poor HDLs could occur in vivo during reverse cholesterol transport (59). Smaller pre $\beta$ 1-HDLs, containing an apoA-I conformation that makes the particle highly efficient at lipid removal, could solubilize lipids from the cell membrane, acquiring a new, larger conformation prone to desorption and further metabolism (59). The binding of the rHDL to the membrane calls for further detailed kinetics studies that may use the high spatial and time resolution provided by scanning FCS (60) and raster image correlation spectroscopy techniques (61).

The use of M $\beta$ CD as an alternative cholesterol acceptor leads to another important observation. By comparison of the concentrations used (Fig. 1B, C), rHDLs are  $\sim$ 1,000 times more efficient than M $\beta$ CD at removing cholesterol from POPC/FC GUVs at 25 °C. This observation is important for future studies, because M $\beta$ CD is widely used to remove cholesterol in vivo and can be toxic for some cells as a result of the high concentration needed. HDL particles, on the other hand, even at high concentrations, may not present this problem and may be an alternative tool in these types of studies.

### A model for the transference of cholesterol from coexisting phases


Based on our observations of cholesterol removal from coexisting  $l_o/l_d$  phases, we propose a model for cholesterol removal by rHDL that may be extended to other acceptors.

When cholesterol is distributed between two lipid phases, there is an equilibrium between the cholesterol content in both phases. This equilibrium depends on temperature, the type of lipid in each phase, and the amount of cholesterol present, among other factors (12, 49, 50, 62, 63). If cholesterol content in one of the phases changes, a new equilibrium will be established in seconds that is much faster than the rate at which GP points are taken (Figs. 5, 6A, B). For the two raft-like mixtures studied, rHDLs remove cholesterol from the  $l_d$  phase. To reestablish the equilibrium between the phases, cholesterol mole-

cules would have to move from the  $l_o$  to the  $l_d$  phase. Based on the speed of cholesterol movement between the phases and the speed of the transfer of cholesterol to the rHDL, our results can be explained in two cases.

In case 1, cholesterol is removed from the  $l_d$  phase and could rapidly equilibrate in the two phases according to their respective affinities. Although some lateral cholesterol diffusion could occur to reequilibrate the phases, if the total cholesterol concentration remains high, the  $l_o$  phase do not disassemble. This is the case for the first mixture [DOPC/DPPE/FC (1:1:1)]. Cholesterol is removed from the  $l_d$  phase, with no changes in the area of the  $l_o$  phase, until either the capacity of the HDL particle is reached or the available cholesterol of this phase is depleted.

In case 2, cholesterol is removed from the  $l_d$  phase and could be slowly replenished from the  $l_o$  phase to achieve reequilibration. If the total cholesterol concentration is low, the border of the phase could disassemble before the rest of the phase. This is the case with the second mixture [POPC/SPM/FC (6:1:1)]. As cholesterol is removed from the  $l_d$  phase, the  $l_o$  phase decreases in size as reequilibration occurs (Fig. 6D). We did not see the total disappearance of the  $l_o$  domains, but we expect that higher concentrations of the acceptor will produce such an effect. This part of our model also explains the experiments described recently by Puff et al. (20) using the mixture POPC/SPM/FC (55:5:20) and plasma HDL.

Finally, we show that LAURDAN GP imaging and two-photon microscopy are a powerful combination of techniques, which provide both the high spatial resolution and real-time data acquisition to follow cholesterol removal from different domains simultaneously. This fact suggests the potential for using GP imaging in vivo. The existence of macro domains in vivo has been reported using LAURDAN GP imaging (64), but in general, phase separation is difficult to visualize. Clearly, careful attention must be taken with in vivo studies, in which the phase separation is not as well defined as in artificial systems, especially when removal of cholesterol from one domain can affect not only other domains on the membrane but also cellular storage locales and proteins immersed in the membrane. The combination of two-photon microscopy, GP measurements, and FCS provides a powerful approach to the problem in vitro and in the future could be applied to in vivo studies. 

This research was supported by the Division of Research Resources of the National Institutes of Health (Grant PHS 5 P41 RR-03155).

## REFERENCES

- Mackness, M. I., and P. N. Durrington. 1995. HDL, its enzymes and its potential to influence lipid peroxidation. *Atherosclerosis*. **115**: 243–253.
- Cockerill, G. W., and S. Reed. 1999. High-density lipoprotein: multipotent effects on cells of the vasculature. *Int. Rev. Cytol.* **188**: 257–297.
- Kellner-Weibel, G., S. J. Luke, and G. H. Rothblat. 2003. Cytotoxic cellular cholesterol is selectively removed by apoA-I via ABCA1. *Atherosclerosis*. **171**: 235–243.
- Castro, G., and C. Fielding. 1988. Early incorporation of cell-derived cholesterol into pre-beta-migrating high-density lipoprotein. *Biochemistry*. **27**: 25–29.
- Forte, T., J. Bielicki, R. Goth-Goldstein, J. Selmek, and M. McCall. 1995. Recruitment of cell phospholipids and cholesterol by apolipoproteins A-II and A-I: formation of nascent apolipoprotein-specific HDL that differ in size, phospholipid composition, and reactivity with LCAT. *J. Lipid Res.* **36**: 148–157.
- Oram, J. F., and J. W. Heinecke. 2005. ATP-binding cassette transporter A1: a cell cholesterol exporter that protects against cardiovascular disease. *Physiol. Rev.* **85**: 1343–1372.
- Yokoyama, S. 2006. Assembly of high-density lipoprotein. *Arterioscler. Thromb. Vasc. Biol.* **26**: 20–27.
- Yancey, P. G., A. E. Bortnick, G. Kellner-Weibel, M. de la Llera-Moya, M. C. Phillips, and G. H. Rothblat. 2003. Importance of different pathways of cellular cholesterol efflux. *Arterioscler. Thromb. Vasc. Biol.* **23**: 712–719.
- Rothblat, G. H., M. de la Llera-Moya, and V. Atger. 1999. Cell cholesterol efflux: integration of old and new observations provides new insights. *J. Lipid Res.* **40**: 781–796.
- Phillips, M. C., K. L. Gillote, M. P. Haynes, W. J. Johnson, S. Lund-Katz, and G. H. Rothblat. 1998. Mechanisms of high density lipoprotein-mediated efflux of cholesterol from cell plasma membranes. *Atherosclerosis*. **137**: 13–17.
- Simons, K., and E. Ikonen. 1997. Functional rafts in cell membranes. *Nature*. **387**: 569–572.
- Veatch, S. L., and S. L. Keller. 2003. Separation of liquid phases in giant vesicles of ternary mixtures of phospholipids and cholesterol. *Biophys. J.* **85**: 3074–3083.
- McIntosh, T. J., A. Vidal, and S. A. Simon. 2003. Sorting of lipids and transmembrane peptides between detergent-soluble bilayers and detergent-resistant rafts. *Biophys. J.* **85**: 1656–1666.
- Pralle, A., P. Keller, E. L. Florin, K. Simons, and J. K. Horber. 2000. Sphingolipid-cholesterol rafts diffuse as small entities in the plasma membrane of mammalian cells. *J. Cell Biol.* **148**: 997–1007.
- Tricerri, M. A., A. Agree, K. Behling, S. A. Sanchez, J. Bronski, and A. Jonas. 2001. Arrangement of apolipoprotein A-I in reconstituted high-density lipoprotein disks: an alternative model based on fluorescence resonance energy transfer experiments. *Biochemistry*. **40**: 5065–5074.
- de Beer, M. C., D. M. Durbin, L. Cai, A. Jonas, F. C. de Beer, and D. R. van der Westhuyzen. 2001. Apolipoprotein A-I conformation markedly influences HDL interaction with scavenger receptor BI. *J. Lipid Res.* **42**: 309–313.
- Tricerri, M. A., S. A. Sanchez, C. Arnulphi, D. M. Durbin, E. Gratton, and A. Jonas. 2002. Interaction of apolipoprotein A-I in three different conformations with palmitoyl oleoyl phosphatidylcholine vesicles. *J. Lipid Res.* **43**: 187–197.
- Angelova, M. I., and D. S. Dimitrov. 1986. Liposome electroformation. *Faraday Discuss. Chem. Soc.* **81**: 303–311.
- Angelova, M. I., S. Soleau, P. Meleard, J. F. Faucon, and P. Bothorel. 1992. Preparation of giant vesicles by external fields. Kinetics and application. *Prog. Colloid Polym. Sci.* **89**: 127–131.
- Puff, N., A. Lamaziere, M. Seigneuret, G. Trugnan, and M. I. Angelova. 2005. HDLs induce raft domain vanishing in heterogeneous giant vesicles. *Chem. Phys. Lipids*. **133**: 195–202.
- Bagatolli, L. A., and E. Gratton. 1999. Two-photon fluorescence microscopy observations of shape changes at the phase transition in phospholipid giant unilamellar vesicles. *Biophys. J.* **77**: 2090–2101.
- Veatch, S. L., and S. L. Keller. 2005. Miscibility phase diagrams of giant vesicles containing sphingomyelin. *Phys. Rev. Lett.* **94**: 148101-1–148101-4.
- Bacia, K., P. Schwille, and T. Kurzchalia. 2005. Sterol structure determines the separation of phases and the curvature of the liquid-ordered phase in model membranes. *Proc. Natl. Acad. Sci. USA*. **102**: 3272–3277.
- Sanchez, S. A., Y. Chen, J. D. Muller, E. Gratton, and T. L. Hazlett. 2001. Solution and interface aggregation states of *Crotalus atrox* venom phospholipase A2 by two-photon excitation fluorescence correlation spectroscopy. *Biochemistry*. **40**: 6903–6911.
- Tricerri, M. A., J. D. Toledo, S. A. Sanchez, T. L. Hazlett, E. Gratton, A. Jonas, and H. A. Garda. 2005. Visualization and analysis of apolipoprotein A-I interaction with binary phospholipid bilayers. *J. Lipid Res.* **46**: 669–678.



26. Sanchez, S. A., and E. Gratton. 2005. Lipid-protein interactions revealed by two-photon microscopy and fluorescence correlation spectroscopy. *Acc. Chem. Res.* **38**: 469–477.
27. Leroy, A., and A. Jonas. 1994. Native-like structure and self-association behavior of apolipoprotein A-I in a water/n-propanol solution. *Biochim. Biophys. Acta.* **1212**: 285–294.
28. Haugland, R. P. 1996. Handbook of Fluorescent Probes and Research Chemicals. Molecular Probes, Inc., Eugene, OR.
29. Jonas, A. 1986. Reconstitution of high-density lipoproteins. *Methods Enzymol.* **128**: 553–582.
30. Weber, G., and F. J. Farris. 1979. Synthesis and spectral properties of a hydrophobic fluorescent probe: 2-dimethylamino-6-propionyl-naphthalene. *Biochemistry.* **18**: 3075–3078.
31. Parasassi, T., G. De Stasio, G. Ravagnan, R. M. Rusch, and E. Gratton. 1991. Quantitation of lipid phases in phospholipid vesicles by the generalized polarization of Laurdan fluorescence. *Biophys. J.* **60**: 179–189.
32. Parasassi, T., and E. Gratton. 1995. Membrane lipid domains and dynamics as detected by Laurdan fluorescence. *J. Fluorescence.* **8**: 365–373.
33. Bagatolli, L. A., S. A. Sanchez, T. L. Hazlett, and E. Gratton. 2003. Giant vesicles, Laurdan, and two-photon fluorescence microscopy: evidence of lipid lateral separation in bilayers. *Methods Enzymol.* **360**: 481–500.
34. So, P. T. C., T. French, W. M. Yu, K. M. Berland, C. Y. Dong, and E. Gratton. 1995. Time resolved fluorescence microscopy using two photon excitation. *Bioimaging.* **3**: 49–63.
35. So, P. T. C., T. French, W. M. Yu, K. M. Berland, C. Y. Dong, and E. Gratton. 1996. Two-photon fluorescence microscopy: time-resolved and intensity imaging. In *Fluorescence Imaging Spectroscopy and Microscopy*. X. F. Wang and B. Herman, editors. John Wiley & Sons, New York. 351–374.
36. Sanchez, S. A., L. A. Bagatolli, E. Gratton, and T. L. Hazlett. 2002. A two-photon view of an enzyme at work: *Crotalus atrox* venom PLA2 interaction with single-lipid and mixed-lipid giant unilamellar vesicles. *Biophys. J.* **82**: 2232–2243.
37. Berland, K. M., P. T. C. So, and E. Gratton. 1995. Two-photon fluorescence correlation spectroscopy: method and applications to the intracellular environment. *Biophys. J.* **68**: 694–701.
38. Thompson, N. L. 1991. Fluorescence correlation spectroscopy. In *Topics in Fluorescence Spectroscopy*. J. R. Lakowicz, editor. Plenum Press, New York. 337–378.
39. Chen, Y., J. D. Muller, K. M. Berland, and E. Gratton. 1999. Fluorescence fluctuation spectroscopy. *Methods.* **19**: 234–252.
40. Thompson, N. L., A. M. Lieto, and N. W. Allen. 2002. Recent advances in fluorescence correlation spectroscopy. *Curr. Opin. Struct. Biol.* **12**: 634–641.
41. Levin, M. K., and J. H. Carson. 2004. Fluorescence correlation spectroscopy and quantitative cell biology. *Differentiation.* **72**: 1–10.
42. Muller, J. D., Y. Chen, and E. Gratton. 2000. Resolving heterogeneity on the single molecular level with the photon-counting histogram. *Biophys. J.* **78**: 474–486.
43. Pucadyil, T. J., and A. Chattopadhyay. 2005. Cholesterol modulates the antagonist-binding function of hippocampal serotonin 1A receptors. *Biochim. Biophys. Acta.* **1714**: 35–42.
44. Westermann, M., F. Steiniger, and W. Richter. 2005. Belt-like localisation of caveolin in deep caveolae and its re-distribution after cholesterol depletion. *Histochem. Cell Biol.* **123**: 613–620.
45. Veatch, S. L., I. V. Polozov, K. Gawrisch, and S. L. Keller. 2004. Liquid domains in vesicles investigated by NMR and fluorescence microscopy. *Biophys. J.* **86**: 2910–2922.
46. de la Serna, J. B., J. Perez-Gil, A. Simonsen, and L. Bagatolli. 2004. Cholesterol rules: direct observation of the coexistence of two fluid phases in native pulmonary surfactant membranes at physiological temperatures. *J. Biol. Chem.* **279**: 40715–40722.
47. Thewalt, J. L., and M. Bloom. 1992. Phosphatidylcholine: cholesterol phase diagrams. *Biophys. J.* **63**: 1176–1181.
48. de Almeida, R. F. M., A. Fedorov, and M. Prieto. 2003. Sphingomyelin/phosphatidylcholine/cholesterol phase diagram: boundaries and composition of lipid rafts. *Biophys. J.* **85**: 2406–2416.
49. Veatch, S. L., and S. L. Keller. 2002. Organization in lipid membranes containing cholesterol. *Phys. Rev. Lett.* **89**: 268101-1–268101-4.
50. Rothblat, G. H., F. H. Mahlberg, W. J. Johnson, and M. C. Phillips. 1992. Apolipoproteins, membrane cholesterol domains, and the regulation of cholesterol efflux. *J. Lipid Res.* **33**: 1091–1097.
51. Needham, D., T. J. McIntosh, and E. Evans. 1988. Thermomechanical and transition properties of dimyristoylphosphatidylcholine/cholesterol bilayers. *Biochemistry.* **27**: 4668–4673.
52. Brown, R. E. 1998. Sphingolipid organization in biomembranes: what physical studies of model membranes reveal. *J. Cell Sci.* **111**: 1–9.
53. Sankaram, M. B., and T. E. Thompson. 1990. Modulation of phospholipid acyl chain order by cholesterol. A solid-state deuterium nuclear magnetic resonance study. *Biochemistry.* **29**: 10676–10684.
54. Sankaram, M. B., and T. E. Thompson. 1991. Cholesterol-induced fluid-phase immiscibility in membranes. *Proc. Natl. Acad. Sci. USA.* **88**: 8686–8690.
55. Harris, J. S., D. E. Epps, S. R. Davio, and F. J. Kezdy. 1995. Evidence for transbilayer, tail-to-tail cholesterol dimers in dipalmitoylglycerophosphocholine liposomes. *Biochemistry.* **34**: 3851–3857.
56. Christian, A. E., M. P. Haynes, M. C. Phillips, and G. H. Rothblat. 1997. Use of cyclodextrins for manipulating cellular cholesterol content. *J. Lipid Res.* **38**: 2264–2272.
57. Yancey, P. G., W. V. Rodriguez, E. P. C. Kilsdonk, G. W. Stoudt, W. J. Johnson, M. C. Phillips, and G. H. Rothblat. 1996. Cellular cholesterol efflux mediated by cyclodextrins: demonstration of kinetic pools and mechanism of efflux. *J. Biol. Chem.* **271**: 16026–16034.
58. Phillips, M. C., W. J. Johnson, and G. H. Rothblat. 1987. Mechanisms and consequences of cellular cholesterol exchange and transfer. *Biochim. Biophys. Acta.* **906**: 223–276.
59. Tricerri, A., B. Corsico, J. D. Toledo, H. A. Garda, and R. R. Brenner. 1998. Conformation of apolipoprotein A-I in reconstituted lipoprotein particles and particle-membrane interaction: effect of cholesterol. *Biochim. Biophys. Acta.* **1391**: 67–78.
60. Ruan, Q., M. A. Cheng, M. Levi, E. Gratton, and W. W. Mantulin. 2004. Spatial-temporal studies of membrane dynamics: scanning fluorescence correlation spectroscopy (SFCS). *Biophys. J.* **87**: 1260–1267.
61. Digman, M. A., P. Sengupta, P. W. Wiseman, C. M. Brown, A. R. Horwitz, and E. Gratton. 2005. Fluctuation correlation spectroscopy with a laser-scanning microscope: exploiting the hidden time structure. *Biophys. J.* **88**: 33–36.
62. Scheidt, H. A., D. Huster, and K. Gawrisch. 2005. Diffusion of cholesterol and its precursors in lipid membranes studied by  $^1\text{H}$  pulsed field gradient magic angle spinning NMR. *Biophys. J.* **89**: 2504–2512.
63. Oradd, G., P. W. Westerman, and G. Lindblom. 2005. Lateral diffusion coefficients of separate lipid species in a ternary raft-forming bilayer: a Pfg-NMR multinuclear study. *Biophys. J.* **89**: 315–320.
64. Gaus, K., E. Gratton, E. P. W. Kable, A. S. Jones, I. Gelissen, L. Kritharides, and W. Jessup. 2003. Visualizing lipid structure and raft domains in living cells with two-photon microscopy. *Proc. Natl. Acad. Sci. USA.* **100**: 15554–15559.